Journal of System Design and Dynamics

Vol.3, No.3, 2009

Design and Stability Analysis of a 3D Rimless Wheel with Flat Feet and Ankle Springs*

Terumasa NARUKAWA**, Masaki TAKAHASHI*** and Kazuo YOSHIDA†

** Keio University, Center for Education and Research of Symbiotic, Safe and Secure System Design
4–1–1 Hiyoshi, Kohoku-ku, Yokohama 223–8526, Japan
E-mail: narukawa@2003.jukuin.keio.ac.jp

*** Keio University, the Department of System Design Engineering
3–14–1 Hiyoshi, Kohoku-ku, Yokohama 223–8522, Japan
E-mail: takahashi@sd.keio.ac.jp

† Keio University, the Department of System Design Engineering
3–14–1 Hiyoshi, Kohoku-ku, Yokohama 223–8522, Japan

Abstract

A two-dimensional rimless wheel provides a simple model of bipedal walking. The motion of the rimless wheel is stable, and this particular property has clarified the fundamental role of a swing leg in planar bipedal walking that addresses the problem of falling forward. In this paper, a three-dimensional rimless wheel is investigated as a simple model of three-dimensional bipedal walking. The 3D rimless wheel model is useful in understanding the essential dynamics of 3D bipedal locomotion. The model consists of two rimless wheels connected by a link at the center of the wheels, and flat feet connected to the spokes with springs. The first numerical stability studies indicated that the motion of the 3D rimless wheel could be unstable; however, numerical simulations and experimental results showed that for a given slope and physical parameters, including the spring constant at the ankles, a stable motion is obtained. This indicates the usefulness of ankle springs in providing stable bipedal locomotion in three-dimensions.

Key words : Rimless Wheel, 3D, Springs, Experiments, Stability Analysis, Passive Dynamic Walking, Mechanism, Legged Locomotion

1. Introduction

Study of several simple models of bipedal locomotion has shown the usefulness of investigating the simple models to understand the essential dynamics of bipedal locomotion, e.g. (1)–(7). One of the simplest bipedal locomotion model is a rimless wheel[8),(9)] as shown in Fig. 1(a). An ideal wheel can move steadily on a level ground. Its motion is not as different from that of a bipedal locomotion as one might first imagine. We can obtain a rimless wheel by simply removing the rim from the wheel, leaving a number of the spokes, i.e., legs, at fixed angles as shown in Fig. 2. The rimless wheel has been studied to understand the bipedal locomotion. The rimless wheel model captures two main features of biped locomotion, of which one is the stance leg motion. The motion of a spoke that comes in contact with the ground corresponds to the stance leg motion in biped locomotion, which acts as an inverted pendulum motion. The other feature is the heel strike when the swing leg touches the ground. The stance leg is exchanged during the impact phase, which prevents the biped from falling forward. The role of the heel strike, which leads to the fundamental stability mechanism, can be explained by the rimless wheel model[(9)–(11)]. Although kinetic energy is lost each time a new spoke impacts the slope, some kinetic energy is gained from the movement down the slope. The rimless wheel exhibits a periodic motion if the energy loss and gain are equal. If they are not equal, an energy balance mechanism comes into play. For instance, if the rimless wheel moves faster than the stable motion, larger energy loss than the stable motion occurs.

*Received 18 Mar., 2009 (No. 09-0114)
[DOI: 10.1299/jsdd.3.258]

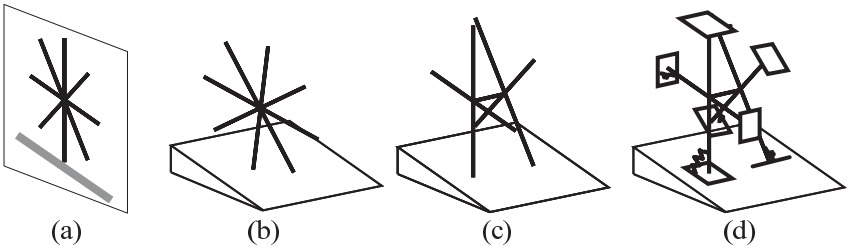

Fig. 1 Rimless wheels. (a) The original rimless wheel model. (b) A rimless wheel including three-dimensional motion. (c) A 3D rimless wheel which has finite hip width. (d) Our 3D rimless wheel, which has flat feet and ankle springs.

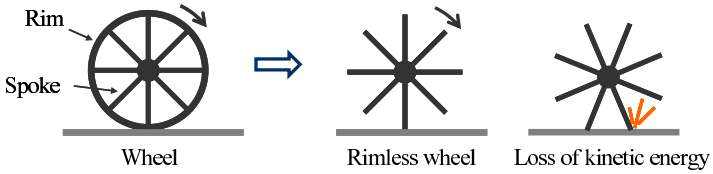

Fig. 2 Wheel vs. rimless wheel.

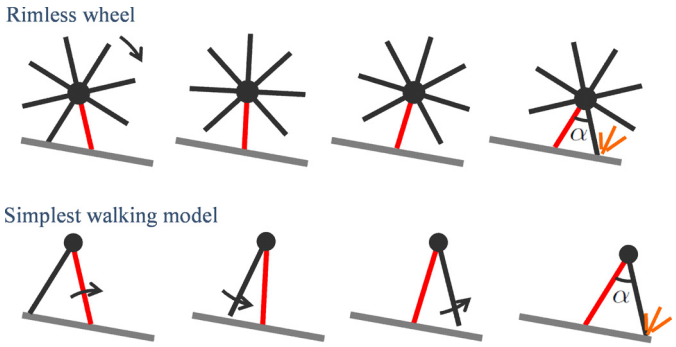

Fig. 3 Rimless wheel vs. simplest walking.

This reduces the speed because the energy gain per step remains constant. The rimless wheel will asymptotically go back to the stable motion. The rimless wheel has an equilibrium motion for a given slope angle[9),(10)]. The stable region for a rimless wheel is very large[12)]. This remarkable feature is used to strengthen the stability of passive walkers[13)] and powered biped walkers[12)] as indicated in Fig. 3. Wisse et al. concluded that a planar biped will never fall forward if the swing leg is stepped quickly in front of the stance leg[12)].

Coleman et al. studied the motion of a rimless wheel in three-dimensional plane as shown in Fig. 1(b). Smith and Berkemeier[14)] extended the rimless wheel to a three-dimensional version which consists of two rimless spoked wheels connected by a link at the center of the wheels as shown in Fig. 1(c). The two rimless wheel is connected so that alternate sides of the spoked wheel touches the ground. The 3D rimless wheel was used to understand 3D bipedal locomotion with hip width and leg separation. However they only studied the motion of the 3D rimless wheel through numerical simulations and the angle between spokes is $\pi/8$ rad which is small compared to passive walking and normal human walking[9)].

In this paper, the angle between spokes is set to be $\pi/4$ rad which is large enough compared to the passive walking and human walking. The main feature of this study is the ankle and foot design as shown in Fig. 1(d). Flat feet are added to the 3D rimless wheel. The flat feet are connected to the legs with the ankle joints which have two degrees of freedom for roll and pitch motion. Roll is rotation about an axis in the direction of walking. Pitch is rotation about an axis perpendicular to the direction of walking. The authors have experimentally

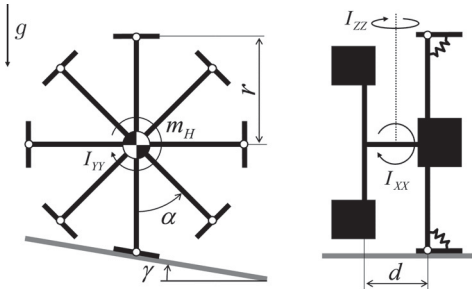

Fig. 4 Model of 3D rimless wheel with flat feet and ankle springs.

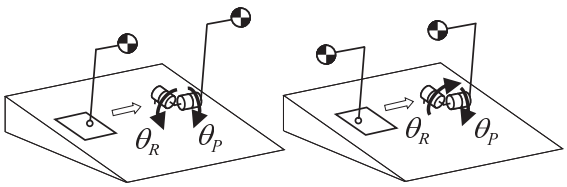

Fig. 5 An approximate model of the flat feet and the legs connected by joints with two degrees of freedom. For clarity, only the stance leg is shown.

shown that this assembly helps a 3D passive biped walker to achieve sufficient friction torque from the ground to avoid unstable yaw motions[15),(16)]. However, the effectiveness of the torsional spring stiffness at the ankle joint in providing stable periodic motion has not been extensively investigated. We investigate the effects of the torsional spring stiffness at ankle joints on the stable motion of 3D passive walking. In this study, we use a three-dimensional rimless wheel, which is a simple model of 3D passive walking, to show that the addition of ankle springs helps obtain a stable motion. We have already performed preliminary numerical simulations on the 3D rimless wheel[17]. In this paper, we describe the detailed stability analysis and experiments on the 3D rimless wheel. Numerical simulations show that the motion of the 3D rimless wheel is unstable without ankle springs. Then the effect of ankle spring for roll motion is investigated through numerical simulations. Ankle springs are added to the 3D rimless wheel to obtain stable motion. When appropriate value of the spring constant is set, the 3D rimless wheel exhibits stable motion. Experimental studies are performed to show the usefulness of the proposed method. Experimental result shows that rebound occurs when the foot impacts with the ground leading to unstable motion. The ankle spring for pitch motion is added to avoid the rebound. Finally, experimental results show that the flat feet and ankle springs for roll and pitch motion enables the 3D rimless wheel to be stable motion. The results indicate that flat feet and ankle springs are useful to obtain stable walking in 3D bipedal locomotion.

2. Modeling of 3D Rimless Wheel

2.1. Equations of Motion

Figure 4 shows the 3D rimless wheel model investigated in this paper. The model of the 3D rimless wheel consists of two rimless spoked wheels connected by a link at the center of the wheels. In Fig. 4, m_H is the total mass of the 3D rimless wheel, r is the length of a leg, d is the distance between the rimless wheels, α is the angle between two adjacent legs on the opposite side of the wheels, I_{XX} and I_{ZZ} are moments of inertia about the axes perpendicular to the joint at the center of the wheels and passing through the center of mass, I_{YY} is the moment of inertia about the axis along the joint at the center of the wheels and passing through the center of mass, and g is the gravitational acceleration. In this paper, flat feet are connected to the spoke ends to gain sufficient friction torque against unstable yaw motion. Torsional springs are also attached to the joints between the feet and the legs. The model of the 3D rimless wheel is simplified as shown in Fig. 5 because numerical simulations

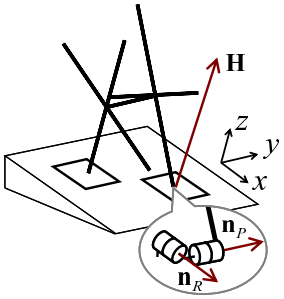

Fig. 6 Conservation of total angular momentum of 3D rimless wheel about the ankle joint.

of the 3D rimless wheel is difficult, mainly due to collisions between the swing foot and the ground, and the frictional phenomena between the stance foot and the ground. The feet except the stance foot are considered to be a point foot in order to make the motion of the feet negligible. The stance foot and ankle is modeled as the point foot with the two degrees of freedom for roll angle and pitch angle between the ground and the foot. The effect of the spring stiffness for the roll motion is investigated in numerical simulations. The effect for the pitch motion is investigated through experiments of a physical 3D rimless wheel.

The dynamic model of the 3D rimless wheel is obtained by the Euler-Lagrange equations as

$$M(\boldsymbol{\theta})\ddot{\boldsymbol{\theta}} + C\left(\boldsymbol{\theta}, \dot{\boldsymbol{\theta}}\right)\dot{\boldsymbol{\theta}} + G(\boldsymbol{\theta}) = \begin{bmatrix} T \\ 0 \end{bmatrix} \tag{1}$$

where M is the mass-inertia matrix, C is the Coriolis matrix, G is the gravity term, and $\boldsymbol{\theta} = \begin{bmatrix} \theta_R & \theta_P \end{bmatrix}^T$. θ_R is the roll angle of the stance leg. θ_P is the pitch angle of the stance leg as shown in Fig. 5. T is the torque applied by the springs for the roll motion. T is calculated as $T = -k_r\theta_R$ where k_r is the torsional spring constant. The matrices are as follows.

$$M = \begin{bmatrix} M_{11} & M_{12} \\ M_{12} & M_{22} \end{bmatrix}, M_{11} = m_H\left(\tfrac{1}{4}d^2 + r^2\cos^2\theta_P\right) + I_{XX}\cos^2\theta_P + I_{ZZ}\sin^2\theta_P,$$

$$M_{12} = -\tfrac{1}{2}m_H dr\sin\theta_P, M_{22} = m_H r^2 + I_{YY},$$

$$C = \begin{bmatrix} C_{11} & C_{12} \\ C_{21} & 0 \end{bmatrix}, C_{11} = \left(-m_H r^2 - I_{XX} + I_{ZZ}\right)\dot{\theta}_P\sin\theta_P\cos\theta_P,$$

$$C_{12} = \left(\dot{\theta}_R\sin\theta_P\left(-m_H r^2 - I_{XX} + I_{ZZ}\right) - \tfrac{1}{2}m_H dr\dot{\theta}_P\right)\cos\theta_P,$$

$$C_{21} = \left(m_H r^2 + I_{XX} - I_{ZZ}\right)\dot{\theta}_R\sin\theta_P\cos\theta_P,$$

$$G = \begin{bmatrix} m_H g\cos\gamma\left(\tfrac{1}{2}d\cos\theta_R - r\sin\theta_R\cos\theta_P\right) \\ -m_H gr\left(\sin\gamma\cos\theta_P + \cos\gamma\cos\theta_R\sin\theta_P\right) \end{bmatrix}.$$

2.2. Impact equations

The impact assumptions are the same as those for passive walkers[9] and rimless wheels [10), (14]. The impact between the swing foot and the ground is assumed to be inelastic and without slipping leading to an instantaneous impulse applied at the point of impact, which causes a discontinuous change in velocity. During impact, the orientation of the rimless wheel remains unchanged. It is also assumed that no such impulse occurs at the trailing leg. The

Table 1 Physical Parameters of 3D rimless wheel. The value of d is determined by the stability analysis (see Section 3)

Parameter	Unit	Value	Parameter	Unit	Value
m_H	kg	3.41	I_{XX}	$\mathrm{kg \cdot m^2}$	0.13
r	m	0.36	I_{YY}	$\mathrm{kg \cdot m^2}$	0.23
d	m	0.16	I_{ZZ}	$\mathrm{kg \cdot m^2}$	0.13
α	rad	$\pi/4$	g	$\mathrm{m/s^2}$	9.8

Fig. 7 Our physical 3D rimless wheel with flat feet and ankle springs.

conservation law applied to the angular momentum during impact leads to the relationship between the pre- and post-impact angular velocities.

Two equations for conservation of angular momentum are needed to fully determine the two post-impact angular velocities. Denoting the angular momentum of the whole 3D rimless wheel about the ankle joint of the leading leg as the vector $\boldsymbol{H}$, two components of this quantity are conserved.

$$\boldsymbol{H}^+\left(\boldsymbol{\theta}^+, \dot{\boldsymbol{\theta}}^+\right) \cdot \boldsymbol{n}_R = \boldsymbol{H}^-\left(\boldsymbol{\theta}^-, \dot{\boldsymbol{\theta}}^-\right) \cdot \boldsymbol{n}_R, \tag{2}$$

$$\boldsymbol{H}^+\left(\boldsymbol{\theta}^+, \dot{\boldsymbol{\theta}}^+\right) \cdot \boldsymbol{n}_P = \boldsymbol{H}^-\left(\boldsymbol{\theta}^-, \dot{\boldsymbol{\theta}}^-\right) \cdot \boldsymbol{n}_P \tag{3}$$

where the superscripts "-" and "+" indicate pre and post-impact values, respectively. Figure 6 shows the direction of $\boldsymbol{H}$, $\boldsymbol{n}_R$, and $\boldsymbol{n}_P$. $\boldsymbol{n}_R$ is the unit vector along the axis of the ankle joint representing roll motion, $\boldsymbol{n}_P$ is the unit vector along the axis of ankle joint representing pitch motion. Equations (2) and (3) are all linear in $\dot{\boldsymbol{\theta}}$. Then we obtain

$$Q^+\left(\boldsymbol{\theta}^+\right)\dot{\boldsymbol{\theta}}^+ = Q^-\left(\boldsymbol{\theta}^-\right)\dot{\boldsymbol{\theta}}^-. \tag{4}$$

Note that the pre- and post-impact matrices Q^- and Q^+ are dependent on the orientation of the rimless wheel at impact. The angles are relabeled as

$$\boldsymbol{\theta}^+ = \boldsymbol{S}_R\left(\boldsymbol{\theta}^-\right) \tag{5}$$

where

$$\boldsymbol{S}_R = \begin{bmatrix} -\theta_R^- \\ \theta_P^- - \alpha \end{bmatrix}.$$

From Eqs. (4) and (5), we obtain the angular velocities of post-impact as

$$\dot{\boldsymbol{\theta}}^+ = Q^+\left(\boldsymbol{\theta}^+\right)^{-1} Q^-\left(\boldsymbol{\theta}^-\right)\dot{\boldsymbol{\theta}}^- \tag{6}$$

$$= Q^+\left(\boldsymbol{S}_R\left(\boldsymbol{\theta}^-\right)\right)^{-1} Q^-\left(\boldsymbol{\theta}^-\right)\dot{\boldsymbol{\theta}}^- \tag{7}$$

$$= S\left(\boldsymbol{\theta}^-\right)\dot{\boldsymbol{\theta}}^- \tag{8}$$

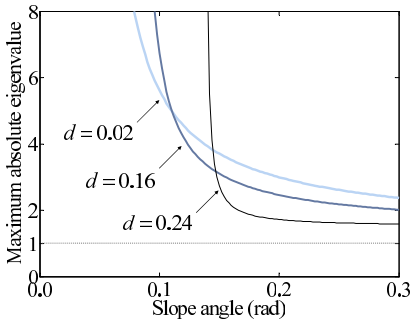

Fig. 8 The maximum absolute eigenvalue vs. slope angle

where

$$S(\theta^-) = \frac{1}{S_D}\begin{bmatrix} S_{11} & S_{12} \\ S_{21} & S_{22} \end{bmatrix}, \tag{9}$$

$$S_{11} = (a_1 + I_{YY})(a_2 - I_{XX} - a_1 c_P (s_P s_A + c_P c_A)) + \tfrac{1}{2} a_1 a_2 (c_{2P2A} - 1),$$

$$S_{12} = -\tfrac{1}{2} m_H r d ((a_1 + I_{YY}) s_P + (a_1 c_A + I_{YY}) s_{PA}),$$

$$S_{21} = m_H r d \left(s_{PA}\left(I_{XX} + \tfrac{1}{4} a_1 \left(\tfrac{1}{2} + c_{2PA} + c_A\right)\right) + \tfrac{1}{8} a_1 s_{3P3A}\right),$$

$$S_{22} = \tfrac{1}{2} a_1 a_2 (c_A + c_{2PA}) + a_1 \left(a_1 c_A {c_{PA}}^2 + c_A I_{XX} + {c_{PA}}^2 I_{YY}\right) + I_{XX} I_{YY} + a_2 I_{YY},$$

$$S_D = a_1 {c_{PA}}^2 (a_1 + a_2 + I_{YY}) + a_1 I_{XX} + a_2 I_{YY} + I_{XX} I_{YY},$$

$$a_1 = m_H r^2,\ a_2 = \tfrac{1}{4} m_H d^2,\ s_A = \sin\alpha,\ c_A = \cos\alpha,\ s_P = \sin\theta_P^-,\ c_P = \cos\theta_P^-,$$

$$s_{PA} = \sin(-\theta_P^- + \alpha),\ c_{PA} = \cos(-\theta_P^- + \alpha),\ c_{2PA} = \cos(-2\theta_P^- + \alpha),$$

$$c_{2P2A} = \cos(-2\theta_P^- + 2\alpha),\ s_{3P3A} = \sin(-3\theta_P^- + 3\alpha).$$

3. Stability Analysis

The stability analysis of the motion is performed using a Poincaré map, which McGeer called as a stride function[9]. The Poincaré section is chosen as the state just after the impact of the leading spoke. Table 1 shows the values of the parameters used for the stability analysis which are that of the physical 3D rimless wheel as shown in Fig. 7. The hip width d is changed to find stable motion. A fixed point is searched using the Newton-Raphson method [9],[18]. When the fixed point is found, the Jacobian matrix of the Poincaré map about the fixed point is calculated numerically and the eigenvalues of the Jacobian matrix are obtained. If the maximum absolute eigenvalue is less than one, the periodic motion is locally however asymptotically stable.

As a first step, the conditions of stable motion are searched by changing the hip width from 0.02 m to 0.24 m, and the slope angle from 0 rad to 0.3 rad while the spring constant is zero, i.e. the spring is removed. In the search, the conditions of the stable motion are not found. The all maximum absolute eigenvalues are larger than one. Figure 8 shows the examples of the transition of the maximum absolute eigenvalue with changing the slope angle and hip width while the spring constant is zero. In the stability analysis we can conclude that the stable motion is not obtained when the spring is removed.

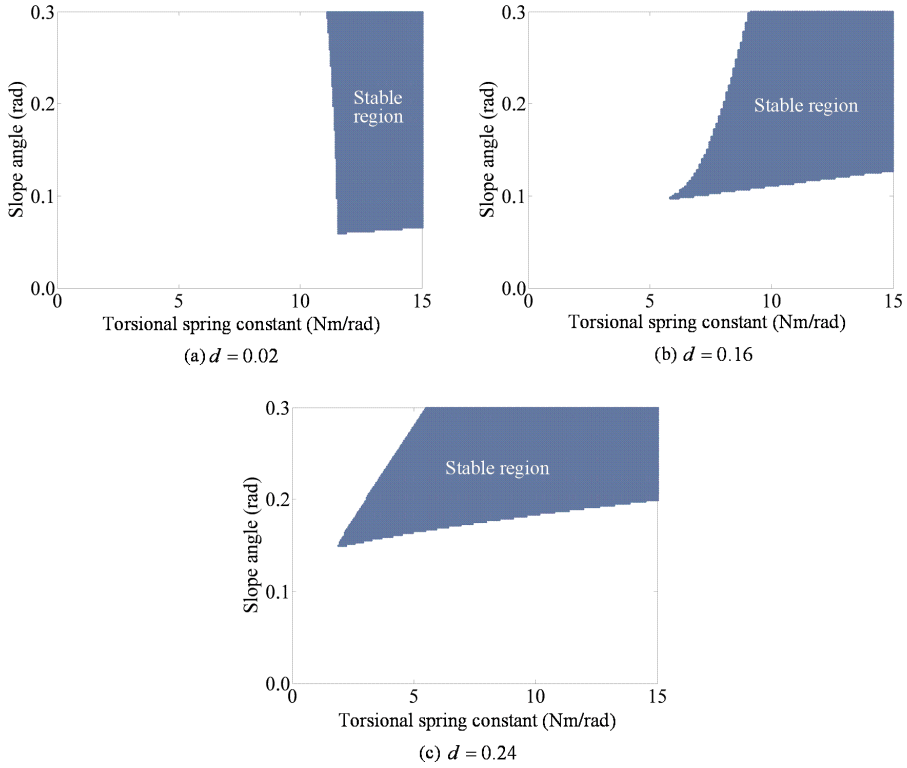

Fig. 9 Stable region with torsional spring constant.

Next, the springs for roll motion are attached to the 3D rimless wheel. The parameters which enable the wheel to exhibit stable motion are searched by changing the hip width from 0.02 m to 0.24 m, and the slope angle from 0 rad to 0.3 rad and the torsional spring constant from 0.5 Nm/rad to 15 Nm/rad. The ranges of the search are the same as the previous one except that the spring stiffness are introduced at the roll joint of the stance ankle. Figure 9 shows the stable region found through the search with the hip width of 0.02, 0.16, and 0.24 m. From Fig 9, it is shown that the stable motion is obtained when the spring stiffness is sufficiently large and the stable region is changed depending on the hip width. The minimum value of the slope angle which shows the stable motion increases with the increase of hip width. The minimum value of the spring constant which shows the stable motion decreases with the increase of hip width. However, it is shown that, with any value of the hip width in the search, shallow angles and small values of the spring constant cannot enable the rimless wheel to be stable. In fact periodic stable or unstable motions are not found when the wheel move on a shallow slope. It is easily explained by using analogy of a 2D rimless wheel[10]. Therefore it is not important that the stability motion is not found at a small slope angle. The important results is that the 3D rimless wheel is not stable even if the slope angle is increased when the springs are removed. This is very different from the 2D rimless wheel which is always stable if the slope angle is large enough to the inter-leg angles of the wheel. The simulation results show that one solution to obtain stable motion of 3D rimless wheel is spring stiffness at the roll angle.

4. Physical 3D Rimless Wheel

4.1. Design and Construction of 3D Rimless Wheel

Figure 7 shows the physical rimless wheel. Figure 10 shows the foot and ankle of the 3D rimless wheel. The flat foot and the leg are joined by a universal joint that has two degrees of freedom. Sponge sheets are attached to the soles of the feet to increase friction. The torsional spring effect is realized by using a pair of tension springs. Tension springs are attached to the

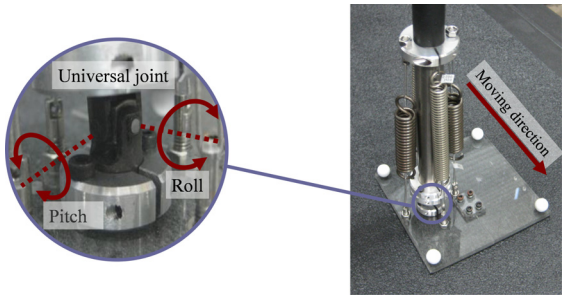

Fig. 10 Foot and ankle design. The flat foot and the leg are joined by a universal joint that has two degrees of freedom. Tension springs are attached to the feet. Sponge sheets are attached to the soles of the feet.

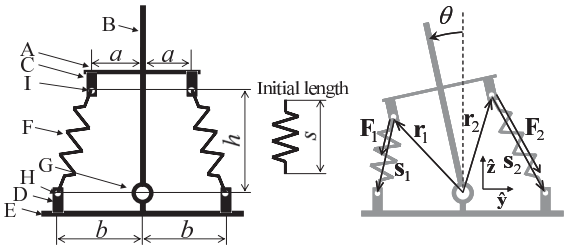

Fig. 11 Model of foot and ankle springs. "A" is rigidly attached to the leg "B." Spring posts "C" are attached to "A." Spring posts "D" are attached to the foot "E." Springs "F" are connected to "A" and "E" through "C" and "D," respectively. The ankle joint "G" and the connected point "H" are attached to the foot at the same height. *a* is the distance between "B" and "C," *b* is the distance between "G" and "H," and *h* is the distance between the connected points "H" and "I" of the spring along the leg. The torque about the ankle joint is produced by the springs.

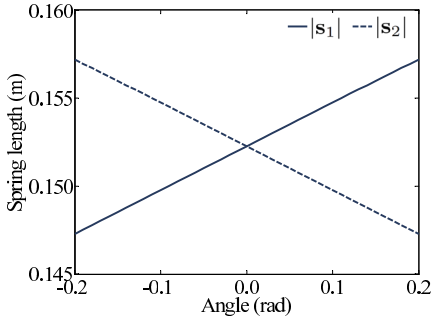

Fig. 12 The relationship between the roll angle and the spring length.

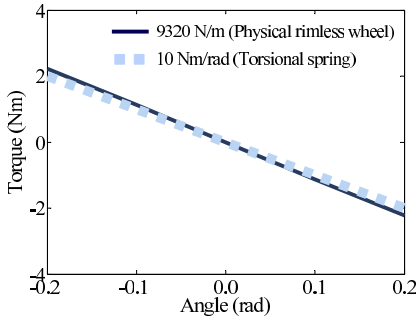

Fig. 13 The relationship between the roll angle and the torque applied by the springs.

Table 2 Parameters of foot and ankle design of 3D passive walker. The spring stiffness for pitch motion is introduced to reduce the rebound motion when the leading leg impacts with the ground (See Section 4.2).

Parameter	Unit	Value (roll)	Value (pitch)
a	m	0.016	0.016
b	m	0.025	0.025
h	m	0.152	0.164
s	m	0.144	0.152
k	N/m	9320	3920

feet and the legs to produce torque about the joint. The effect of the tension springs is simply calculated as follows[16]. First we assume that the roll and pitch motion are each isolated. The

roll or pitch motion is described by the following expressions and shown in Fig. 11. The forces produced by the springs are

$$|\boldsymbol{F}_1| = k\,(|\boldsymbol{s}_1| - s)\,, \tag{10}$$

$$|\boldsymbol{F}_2| = k\,(|\boldsymbol{s}_2| - s) \tag{11}$$

where k is the spring constant and s is the initial length of the spring. We assume that the spring force obeys Hooke's law. The torque produced by the spring forces becomes

$$\boldsymbol{T} = \sum_{i=1}^{2} \boldsymbol{r}_i \times \boldsymbol{F}_i = \sum_{i=1}^{2} k\,(|\boldsymbol{s}_i| - s)\,\boldsymbol{r}_i \times \frac{\boldsymbol{s}_i}{|\boldsymbol{s}_i|}. \tag{12}$$

Figure 11 provides the necessary notation. Then

$$\boldsymbol{r}_1 = (-h\sin\theta - a\cos\theta)\,\hat{\boldsymbol{y}} + (h\cos\theta - a\sin\theta)\,\hat{\boldsymbol{z}}, \tag{13}$$

$$\boldsymbol{r}_2 = (-h\sin\theta + a\cos\theta)\,\hat{\boldsymbol{y}} + (h\cos\theta + a\sin\theta)\,\hat{\boldsymbol{z}}, \tag{14}$$

$$\boldsymbol{s}_1 = -\boldsymbol{r}_1 - b\hat{\boldsymbol{y}}, \tag{15}$$

$$\boldsymbol{s}_2 = -\boldsymbol{r}_2 + b\hat{\boldsymbol{y}}. \tag{16}$$

$\hat{\boldsymbol{y}}$ and $\hat{\boldsymbol{z}}$ are the unit vectors shown in Fig. 11. a is the distance between the leg and the spring post attached to the leg, b is the distance between the ankle joint and the spring post attached to the foot, and h is the distance between the connected points on the spring along the leg, as indicated in Fig. 11. Figure 12 shows the length of the springs versus the ankle angle for roll motion. Figure 13 shows the relation between the ankle angle and the torque applied by the springs of 9320 N/m for roll motion compared with the torsional spring of 10 Nm/rad. Table 2 lists the values of the physical parameters of the walker and that are used for calculation in Figs. 12 and 13.

4.2. Experimental Results

The physical rimless wheel moves on a treadmill. The width of the treadmill is 0.4 m, the length is 1.2 m. The torsional spring constant for roll motion is approximately 10 Nm/rad as indicated in Fig. 13. The hip width is 0.16 m. The slope angle is 0.15 rad. In the conditions, it is expected that the 3D rimless wheel exhibits stable motion as shown in Fig. 9(b). The 3D rimless wheel is launched manually by hands.

When the spring constant for pitch motion is negligibly small, the stable motion is not obtained. The cause of unstable motions is the rebound when the leg impacts with the ground. When the rebound occurs the 3D rimless wheel jumps at a short instance and the foot of the stance leg moves like slipping. This disturbance immediately causes the motion to be unstable. In numerical simulations, the impact between the swing foot and the ground is assumed to be inelastic and without slipping. The experimental result indicates that the assumption of the perfect plastic collision is not appropriate when no ankle springs for pitch motion are attached to the legs and the feet.

The spring constant for pitch motion is sets as 3920 N/m to reduce the rebound motion produced on impact. The spring attached to provide pitch motion makes the 3D rimless wheel move faster because the loss in kinetic energy due to the impacts is reduced. The slope angle is adjusted such that the speed of the experimental 3D rimless wheel in the same as that in the numerical simulations in which the spring for pitch motion is absent. The slope angle is reset to 0.08 rad. Under these conditions, the 3D rimless wheel exhibits stable motions, as shown in Fig. 14. Figure 15 shows the set up for recording the motion of the 3D rimless wheel to obtain the pictures shown in Fig. 14. In the most successful result, the 3D rimless wheel moves stably more than 250 steps, 100 seconds in the treadmill. After that, the wheel was stopped because the direction of the wheel is slightly changed leading to move the over

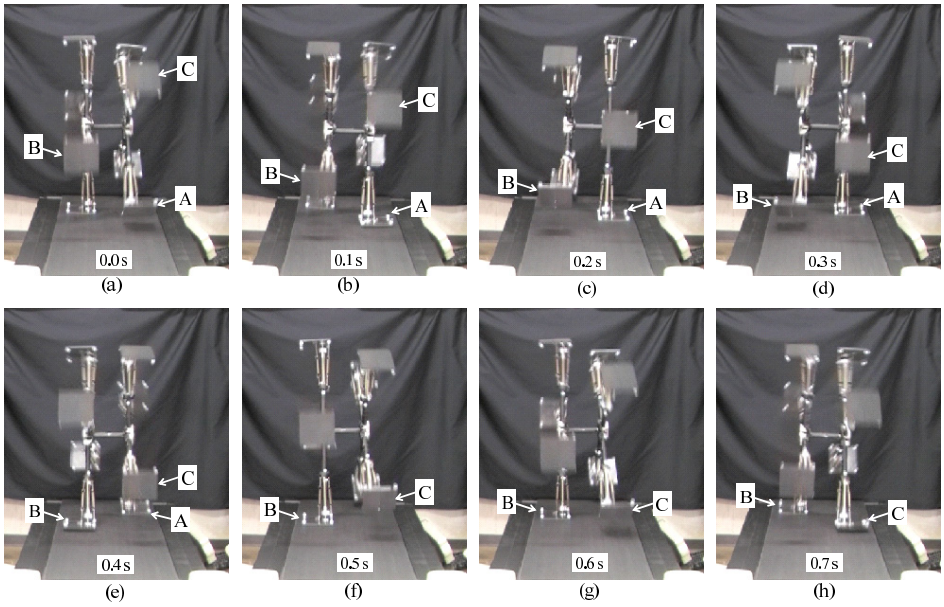

Fig. 14 Photos recorded in a sequence showing stable motion of 3D rimless wheel taking one stride, i.e., two steps. The foot (A) on the left hand side of the wheel, or on the right hand side when viewed from the front, about to touch the ground (a). The foot touching the ground and the stance leg being exchanged (b). One step is complete as the foot (B) on the right hand side of the wheel touching the ground (e). When the foot (C) on the left hand side of the wheel touches the ground, one stride, i.e., two steps, is complete from (b) to (h).

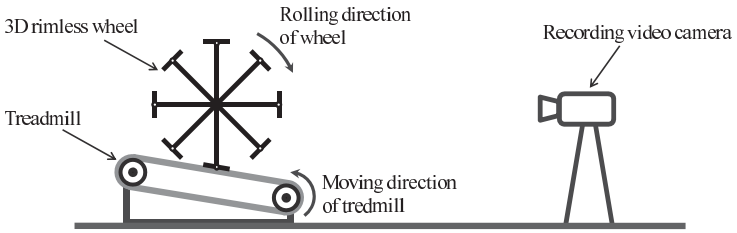

Fig. 15 Set up to record the motion of 3D rimless wheel, the pictures of which are shown in Fig. 14.

side of the treadmill. Figure 16 indicates the motion capture data of the physical 3D rimless wheel between just before the impact and just after the next impact. The motion is captured by two cameras with 120 fps. The locations of the markers at legs and the stance foot are calculated by the images of the cameras. After that the ankle angles for roll and pitch motion are estimated by the relative attitude between the legs and foot. The experimental data shown in Fig. 16 is the average value of 12 stable steps. Figure 16 indicates that the trajectory of the roll angle is almost the same as the numerical simulation. However, the trajectory of the pitch angle is different around impact phase. The difference between the numerical simulation and the experiments results from kicking motions of the stance leg due to the spring effects for pitch motions. The kicking motion of the stance leg is indicated in Fig. 17. In spite of the kicking motion the 3D rimless wheel exhibits stable motion.

5. Conclusions

This paper presents a three-dimensional rimless wheel with flat feet and ankle springs. The three-dimensional rimless wheel, which is a simple model of three-dimensional walking, was used to show the effect of adding ankle springs to obtain a stable motion. Numerical simulations showed that the motion of the 3D rimless wheel was unstable without ankle springs. Then the effect of ankle spring for roll motion is investigated. Numerical simulations showed

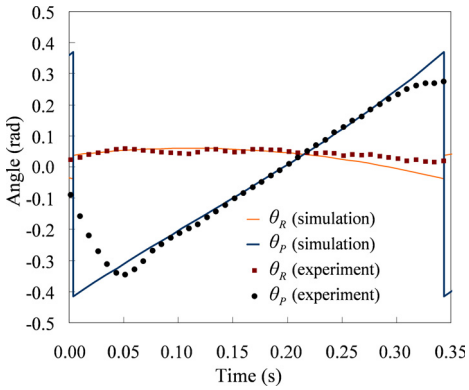

Fig. 16 Comparison between experimental data and numerical simulation.

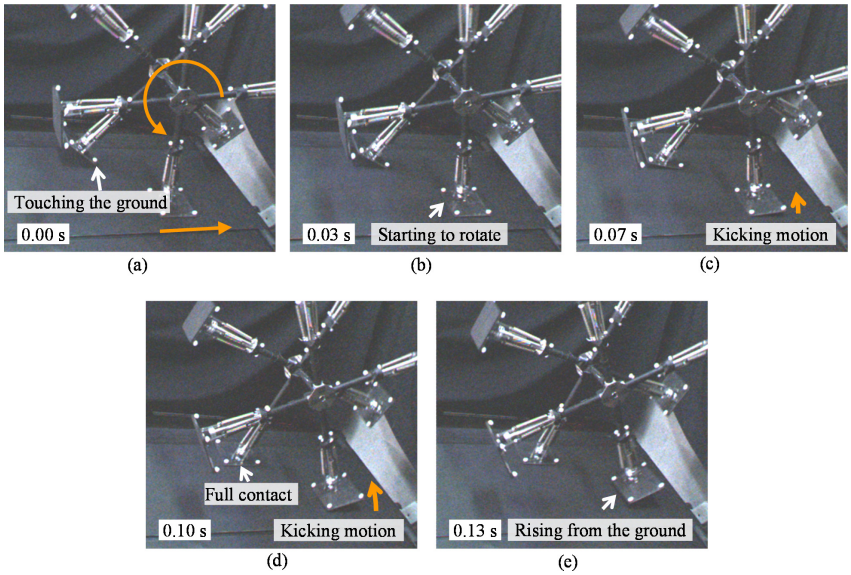

Fig. 17 Kicking motion of 3D rimless wheel achieved by torsional springs attached for pitch motion. The treadmill moves from left to right and the 3D rimless wheel rotates counter-clock wise. The kicking motion of the stance foot occurs before the front foot is in full contact with the ground which then becomes the new stance foot. The heel of the front foot touches the ground (a). The stance foot starts to rotate about its toe (b). The stance foot leaves the ground before the front leg is in full contact with the ground, as indicated in (c). The front leg is in full contact with the ground (d). The pre-stance leg is raised from the ground (e).

that stable motion can be obtained in the presence of ankle springs for roll motion. Experimental result showed that rebound occurred when the foot impacted with the ground. The rebound leaded to unstable motion. The spring stiffness for pitch motion can easily reduce the rebound. When the rebound was reduced, the stable motion was obtained. The results indicate that ankle springs are useful to obtain stable motion in bipedal locomotion in three-dimensions.

Acknowledgments

This work was supported in part by Grant in Aid for the Global Center of Excellence Program for "Center for Education and Research of Symbiotic, Safe and Secure System Design" from the Ministry of Education, Culture, Sports, Science and Technology in Japan.

References

(1) F. Asano, M. Yamakita, N. Kamamichi, and Z.-W. Luo, A novel gait generation for biped walking robots based on mechanical energy constraint, *IEEE Transactions on Robotics and Automation*, Vol. 20, No. 3 (2004), pp. 565-573.

(2) S. Collins, A. Ruina, R. Tedrake, and M. Wisse, Efficient bipedal robots based on passive-dynamic walkers, *Science*, Vol. 307 (2005), pp. 1082-1085.

(3) S. Collins, M. Wisse, and A. Ruina, A three-dimensional passive-dynamic walking robot with two legs and knees, *International Journal of Robotics Research*, Vol. 20, No. 7 (2001), pp. 607-615.

(4) D. G. E. Hobbelen and M. Wisse, Limit cycle walking, In M. Hackel, editor, *Humanoid Robots: Human-like Machines*, I-Tech Education and Publishing, Vienna, Austria, (2007), pp. 277-294.

(5) T. McGeer, Passive dynamic biped catalogue, 1991, In R. Chatila and G. Hirzinger, editors, *Experimental Robotics II: The 2nd International Symposium, Toulouse, France, June 25-27 1991*, Springer-Verlag, (1993), pp. 465-490.

(6) K. Ono, R. Takahashi, and T. Shimada, Self-excited walking of a biped mechanism, *International Journal of Robotics Research*, Vol. 20, No. 12 (2001), pp. 953-966.

(7) M. Srinivasan and A. Ruina, Computer optimization of a minimal biped model discovers walking and running, *Nature*, Vol. 439 (2006) pp.72-75.

(8) R. Margaria, *Biomechanics and Energetics of Muscular Exercise*. Clarendon Press, (1976).

(9) T. McGeer, Passive dynamic walking, *International Journal of Robotics Research*, Vol. 9, No. 2 (1990), pp. 62-82.

(10) M. J. Coleman, A. Chatterjee, and A. Ruina, Motions of a rimless spoked wheel: a simple three-dimensional system with impacts, *Dynamics and Stability of Systems*, Vol. 12, No. 3 (1997), pp. 139-159.

(11) M. Wisse and R. Q. van der Linde, *Delft Pneumatic Bipeds*, Springer-Verlag, Berlin, Heidelberg, (2007).

(12) M. Wisse, A. L. Schwab, R. Q. van der Linde, and F. C. T. van der Helm, How to keep from falling forward: Elementary swing leg action for passive dynamic walkers, *IEEE Transactions on Robotics*, Vol. 21, No. 3 (2005), pp. 393-401.

(13) Y. Ikemata, A. Sano, and H. Fujimoto, A physical principle of gait generation and its stabilization derived from mechanism of fixed point, *Proceedings of the 2006 Conference on International Robotics and Automation*, (2006), pp. 836-841.

(14) A. C. Smith and M. D. Berkemeier, The motion of a finite-width rimless wheel in 3D, *Proceedings of the 1998 IEEE International Conference on Robotics and Automation*, (1998), pp. 2345-2350.

(15) T. Narukawa, K. Yokoyama, M. Takahashi, and K. Yoshida, A simple 3D straight-legged passive walker with flat feet and ankle springs, *IEEE/RSJ International Conference on Intelligent Robots and Systems*, (2008), pp 2952 - 2957.

(16) T. Narukawa, K. Yokoyama, M. Takahashi, and K. Yoshida, Design and construction of a simple 3D straight-legged passive walker with flat feet and ankle springs, *Journal of System Design and Dynamics*, Vol. 3, No. 1 (2009), pp. 1-12.

(17) T. Narukawa, M. Takahashi, and K. Yoshida, The motion of a 3D rimless wheel with flat feet and ankle springs, *Proceedings of the Annual Conference of the Robotics Society of Japan*, (2008), 3B1-07.

(18) M. Garcia, *Stability, scaling, and chaos in passive-dynamic gait models*, PhD thesis, Cornell University, (1999).